Conducting and Piezoresistive Polymer Nanocomposites using Multiwalled Carbon Nanotubes in a Flexible Copolyester: Spectroscopic, Morphological, Mechanical and Electrical Properties

Kedar Nath Dhakal [a,b,c,e], Santosh Khanal [b], Beate Krause [a], Ralf Lach [d], Wolfgang Grellmann [d], Hai Hong Le [a], Amit Das [a], Sven Wießner [a,f], Gert Heinrich [a,g], Jürgen Pionteck [a], Rameshwar Adhikari [b,c,e]

[a] *Leibniz-Institut für Polymerforschung Dresden e.V. (IPF), Hohe Straße 6, 01069, Dresden, Germany*
e-mails: dhakal@ipfdd.de, krause-beate@ipfdd.de, das@ipfdd.de, wiessner@ipfdd.de, gheinrich@ipfdd.de, pionteck@ipfdd.de
[b] *Central Department of Chemistry, Tribhuvan University, Kirtipur, Kathmandu, Nepal*
e-mail: santoshkhanal2003@yahoo.com
[c] *Nepal Polymer Institute (NPI), P. O. Box 24411, Kathmandu, Nepal*
e-mail: kedarchemistry@gmail.com
[d] *Polymer Service GmbH Merseburg (PSM), Eberhard-Leibnitz-Straße 2, 06217, Merseburg, Germany*
e-mails: ralf.lach@psm-merseburg.de, wolfgang.grellmann@psm-merseburg.de
[e] *Research Centre for Applied Science and Technology (RECAST), Tribhuvan University, Kathmandu, Nepal*
e-mail: nepalpolymer@yahoo.com
[f] *Technische Universität Dresden, Institut für Werkstoffwissenschaft, Helmholtzstraße 10, 01069, Dresden, Germany*
[g] *Technische Universität Dresden, Institut für Textilmaschinen und Textile Hochleistungswerkstofftechnik, Hohe Straße 6, 01069, Dresden, Germany*

- Electrical conducting flexible copolyester/MWCNTs nanocomposites with quite low percolation threshold could be prepared.
- Net physical matrix–filler interaction was found to be the binding force for the formation of uniform nanocomposite morphology.
- Piezoresistivity (strain-dependent electrical response) of the nanocomposites was confirmed.
- Strain-sensing applications of the materials at low strain range has been demonstrated.

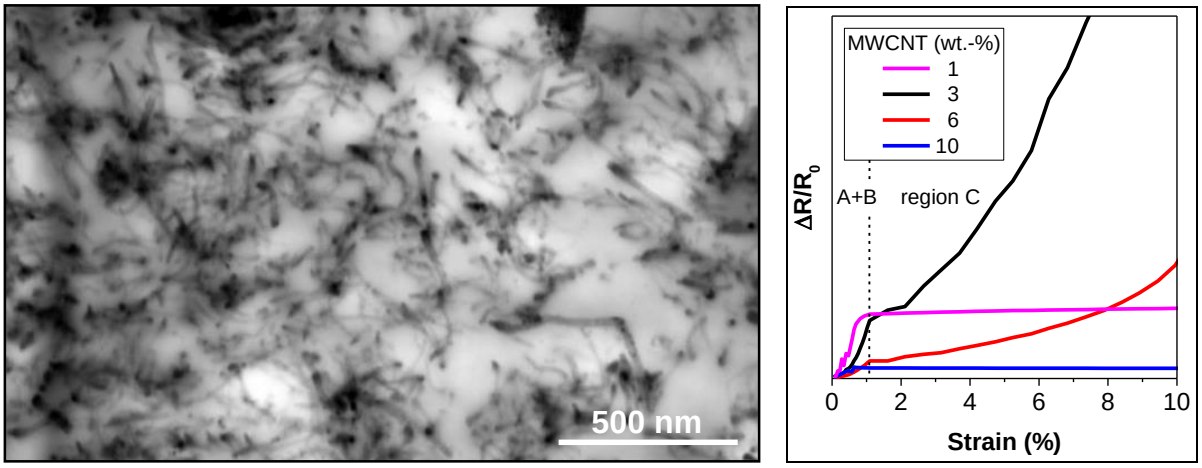

TEM micrograph showing the morphology of a nanocomposite comprising 3 wt.-% of MWCNTs (left) and the relative resistance change ($\Delta R/R_0$) *vs.* strain as a finction of MWCNT content (right).

Abstract

Nanocomposites of multiwalled carbon nanotubes (MWCNTs) with poly(butylene adipate-*co*-terephthalate) (PBAT), a flexible aromatic–aliphatic copolyester, were prepared by melt mixing followed by compression molding to investigate their spectroscopic, morphological, mechanical and electrical properties. Comparison of Fourier transform infrared (FTIR) spectra of the neat polymer matrix and that of the composites showed no difference, implying a physical mixing of the matrix and the filler. The morphological investigation revealed the formation of continuous and interconnected MWCNTs network embedded in the polymer matrix with partial agglomeration. Increasing Martens hardness and indentation modulus and decreasing maximum indentation depth with increasing filler concentration demonstrated the reinforcement of the polymer by the MWCNTs. A volume resistivity of 4.6×10^5 Ω·cm of the materials is achieved by the incorporation of only 1 wt.-% of MWCNTs, which confirmed a quite low percolation threshold (below 1 wt.-%) of the nanotubes. The electrical volume resistivity of the flexible nanocomposites achieved values up to 1.6×10^2 Ω·cm depending on the filler content. The elongation at break of the nanocomposites at 374 % and maximum relative resistance changes ($\Delta R/R_0$) of 20 and 200 at 0.9 % and 7.5 % strains, respectively, were recorded in the nanocomposites (3 wt.-% MWCNTs) within the estimated volume resistivity range. Cyclic strain experiment shows the most stable and homogeneous $\Delta R/R_0$ values at 2–5% strain range. Electrical conductivity and piezoresistivity of the investigated nanocomposites in correlation with mechanical properties and observed morphology make them applicable for low-strain deformation-sensing.

Keywords: *polymer nanocomposites, volume resistivity, electrical conductivity, piezoresistivity, strain-sensing*

1 Introduction

Nanocarbons-based electrical conducting polymer composites whose electrical conductivity is explained on the basis of percolation theory [1] are taken as an alternative to metals and conventional conducting materials. They have attracted the high research interests in both industries and academia [2, 3] as variety of such materials are being used in different fields such as electronics, electrical appliances, construction, sensors, and actuators[4, 5]. They are generally prepared by the incorporation of conducting nanocarbons into polymer matrices or diluting the commercially available master batches of the nanocomposites using the same polymer [1].

Carbon nanotubes (CNTs) are the extensively used nanocarbons because of their high aspect ratio (length-to-diameter ratio, in the range of 100–1000), their outstanding electrical and mechanical properties such as high Young's modulus and high electrical conductivity (similar to that of copper) [1, 6–8]. Melt mixing method is mostly preferred to incorporate the CNTs into polymer matrices to obtain the nanocomposites with desired mechanical and thermal properties although electrical percolation threshold can be slightly increased due to shear induced breaking and shortening of CNTs during melt mixing [9, 10]. Variability of mixing speed, mixing time, shear application and absence of chemicals and solvents are the advantages of this method. The resulting polymer composites undergo an insulator-to-conductor transition at certain filler content called percolation threshold (Φ_C) at which percolation behavior can be observed [11–15]

after which their volume resistivity value gradually levels off and finally becomes constant. A possible lowest percolation threshold is always kept in mind during the preparation of such composite materials with desired physical properties and processability [16, 17]. However, low Φ_C value, enhanced electrical, mechanical and thermal properties in a same material at a time is a difficult task which may become possible only by homogeneous dispersion of individual CNT with a balanced filler–matrix interaction [16-18]. Such a CNT dispersion is limited mainly by their agglomeration carried out by strong van der Waals force of attraction between them and the adhesion of polymer matrix to the filler particles. CNTs agglomeration causes spatial imperfection in composites hampering the desired mechanical properties and reduces the matrix-to-filler stress transfer [8, 19-21].. It also depends on the properties of polymer matrix, physical parameters of CNTs such as aspect ratio, purity, type (single, double or multiwalled), perfection of the walls, surface properties as well as synthetic and processing conditions [3, 22-26].

Φ_C values in the range of 0.0021 to 15 wt.-% has been reported when CNTs are used as conducting fillers in different polymer matrices [13, 25]. Ramasubramaniam *et al.* achieved low percolation between 0.05 and 0.1 wt.-% of filler incorporating single-walled carbon nanotube (SWCNTs) into polystyrene and polycarbonate separately by solution casting method [27]. However, Sandler *et al.* reported ultralow percolation threshold at 0.0025 wt.-% CNTs dispersed in epoxy system [28]. Similarly, Krause *et al.* reported ultralow percolation threshold at 0.04 wt.-% of filler in polyamide 66/MWCNT composites prepared by melt mixing [26].

Increasing demand of flexible, electrical devices, sensors, and actuators provides the scientists with keen research interest of piezoresistive materials [2]. These properties can be developed in flexible, and deformable electrical conducting polymer composites [7, 30-33]. Deformability makes their electrical resistance change by the destruction of conductive network due to mechanical stress while flexibility makes them enable to regenerate the conducting network and regain the same electrical resistance up on removal of stress [30, 33, 34]. Hence, a flexible and deformable polymer matrix with CNTs as conducting filler makes this work possible [12, 31, 35]. In this connection, poly(butylene adipate-*co*-terephthalate) (PBAT), a commercial product of BASF, available as Ecoflex®, an aliphatic–aromatic copolyester of terephthalic acid, adipic acid and 1,4-butanediol is taken as polymer matrix. It is highly flexible (elongation at break = 700 % at 23 °C [36, 37], stretchable, and heat resistant, [38] a soft elastomeric polymer showing excellent processability and mechanical properties [36-39]. Incorporation of CNTs as conductive filler into it has been found to further improve the rheological, electrical, thermal and mechanical properties of PBAT [36, 37, 40].

Hong *et al.* investigated physical characteristics of twin-screw extruded PBAT/MWCNTs nanocomposites of varying composition and found reinforcement in tensile strength and thermal stability [37].

Similarly, Wu developed antibacterial and antistatic MWCNTs/PBAT composites [41]. Ko *et al.* developed MWCNTs/PLA/PBAT nanocomposites using a twin-screw extruder and investigated their rheological and morphological properties [42]. Ding *et al.* prepared CNT/PBAT biocomposites and studied their physical parameters such as creep recovery, stress relaxation, and dynamic shear flow[35]. Amjadi *et al.* prepared thin film of patterned MWCNTs/isopropyl alcohol (IPA) solution and cast into PBAT matrix to apply it as flexible and stretchable strain sensor [12]. Ryu *et al.* used PBAT sheet as a flexible substrate to grow highly oriented CNT fibers and used this material to fabricate an extremely elastic wearable strain sensor [43]. Park *et*

al. developed a wearable strain sensor to monitor human health using CNTs films deposited on a PBAT substrate by spray gun deposition method [44]. Many works regarding to the investigation of strain-sensing behavior of graphene- and graphite-based materials have been reported in literature [34, 45-48]. However, those nanocomposites showed much lower stretchability in comparison to CNT-based strain sensors [35]. This problem can be overcome incorporating CNTs into flexible PBAT whose sensing response can be varied controlling the CNT concentration. It seems from the literature survey that piezoresistive properties of melt-mixed PBAT/MWCNTs nanocomposites are not investigated so far. Thus, investigation of electrical properties, (volume resistivity and piezoresistivity) of the melt-mixed PBAT/MWCNTs nanocomposites along with their morphological and mechanical properties will be the objective of this study. Investigation of strain-sensing behavior of optimized PBAT/MWCNTs will be the new insight.

2 Materials and Methods

2.1 Materials

The polymer matrix used in this work was poly(butylene adipate-*co*-terephthalate) (PBAT), a commercially available aliphatic–aromatic copolyester (molecular weight M_w: 150,000 g/mol, density: 1.27 g/cm^3, melt flow: 4.9 g/10 minutes, melting temperature: 120 °C, glass transition temperature T_g: –30 °C) produced by BASF SE company with its trade name Ecoflex® F BX 7011. Similarly, multiwalled carbon nanotubes (MWCNTs) with trade name Nanocyl NC7000™, a commercially available product of Nanocyl S.A. were used as filler.

2.2 Sample Preparation

PBAT granules and MWCNTs were dried at 80 °C and 120 °C, respectively, for 24 hours using Thermo Scientific™ Vacutherm vacuum heating and drying oven (Thermo Fisher Scientific Inc.). PBAT was then melt-mixed with MWCNTs granules using a twin-screw micro compounder, DSM15 (Xplore Instruments BV, Sittard, The Netherlands) at 180 °C with screw speed of 200 rpm for 5 minutes. The MWCNTs content were 0.5, 1, 3, 6 and 10 wt.-% and the extruded strands obtained from mixing were chopped down. These samples were further dried at 80 °C for 24 hours from which standard circular specimens (discs) of 1 mm thickness and 6.5 cm diameter were prepared by the process of compression moulding using PW40EH hot press (Otto-Paul-Weber GmbH, Remshalden, Germany) at 180 °C (melting time: 1.5 minutes) applying the pressure of 100 kN for 1 minute. Later, dumbbell specimens according to type S3 were cut applying the force (load) of 1 kN. In the following, the PBAT/MWCNTs nanocomposites prepared by melt mixing followed by compression moulding are represented as PBAT / x wt.-% MWCNT, where x stands for the weight fraction of the MWCNTs.

2.3 Characterization Techniques

2.3.1 Spectroscopic Characterization

Fourier Transform Infrared (FTIR) Spectroscopy: FTIR spectra were recorded using Perkin Elmer FTIR-2000 with diamond crystal and attenuated total reflectance (ATR) mode to study the mixing of matrix and filler. Wavenumber range used to record the spectra and the resolution were 500–4000 cm^{-1} and 10 cm^{-1}, respectively.

2.3.2 Morphological Characterization

Scanning Electron Microscopy (SEM): Morphology of cryo-fractured surfaces of the composites was analysed using a scanning electron microscope (Ultra plus microscope, Carl Zeiss GmbH, Oberkochen, Germany). The SEM specimens were prepared by breaking each sample in liquid nitrogen followed by sputter coating of the fracture surfaces by approximately ~80 nm thin film of platinum.

Transmission Electron Microscopy (TEM): Morphology of ultra-thin sections (50 nm thickness) of nanocomposites cut by an ultra-microtome at –100 °C and the CNT dispersion was investigated using transmission electron microscope (TEM, LIBRA-120, Carl-Zeiss GmbH, Oberkochen, Germany) with an acceleration voltage of 120 kV.

2.3.3 Mechanical Characterization

Tensile Test: Dog bone-shaped specimens (5 cm long and 1 mm thick, length and width of the parallel part: 12 mm and 2 mm, respectively) cut from the compression moulded discs were tested using ZwickRoell Z005 universal testing machine (ZwickRoell GmbH & Co. KG, Ulm, Germany) to investigate stress–strain behavior of nanocomposites and that of neat polymer. The specimens used were stretched at a crosshead speed of 1 mm/min in the low-strain range and at 50 mm/min else at 23 °C.

Microindentation Test: Five measurements of loads (F)–indentation depth (h) of each sample were made at different positions of approximately 1×1 cm^2 and 1 mm thick specimen and the average values are reported. The measurements were carried out using a Fischerscope H100C recording microhardness tester (Helmut Fischer GmbH, Sindelfingen, Germany) equipped with a pyramidal Vickers diamond indenter. The indenter was penetrated into the samples applying the force of 300 mN at 23 °C rate of 15 mN/second for both loading and unloading cycles. Average values of hardness parameters i.e. Martens hardness (HM), indentation modulus (E_{IT}) and the works of deformation i.e. elastic work (W_e), plastic work (W_p) and total work ($W_t = W_e + W_p$) were determined from the F–h measurements.

2.3.4 Electrical Characterization

Measurement of Electrical Volume Resistivity: It was measured using Keithley electrometer E6517A (Keithley Instruments, Solon, USA). Pressed plates (for highly resistive samples) and ISO 527-2 standard dumbbell specimens according to type S3 cut from the pressed plates (for conductive samples) were taken for the measurement. The electrometer was combined with Keithley 8009 (Keithley Instruments, Solon, USA) for the samples with volume resistivity $>10^7$ Ω·cm. Similarly, samples with volume resistivity $<10^7$ Ω·cm were measured combining electrometer with a 4-point test fixture having gold electrodes with a distance of 10 mm between the measuring electrodes and a distance of 16 mm between the source electrodes.

Measurement of Piezoresistivity: Piezoresistive behaviour of the composites was measured using Keithley DMM2001 (Keithley Instruments, Solon, USA) electrometer connected to a tensile machine (Zwick/Roell 1456, ZwickRoell GmbH & Co. KG, Ulm, Germany) at 23 °C and 50 % humidity. Tensile machine used here can apply the strain up to 300 % with the force of 1 kN while Keithley 2001 can measure the resistance up to 20 MΩ. The ISO 527-2 standard dumbbell specimens according to type S3 were fixed in stainless steel clamps at their two heads. The two

ends of middle part of the specimens (20 mm long) were connected to Keithley DMM2001 using clamp wires and silver paste was used for better electrical contact and to reduce the contact resistance between clamps and the samples. It was assumed that elongation occurs at the parallel parts of specimens during the test. Previously, resistance of each specimen was measured separately using a multimeter and the value was compared with initial value of resistance (at zero tensile strain) measured by above mentioned device combination. Both of the resistance values measured separately were found to be same. The two devices in combination were clicked at a same time to run both of them together and the resistance change of the samples with increasingly applied tensile strain and mechanical behavior were simultaneously recorded till sample rupture. The relative resistance change ($\Delta R/R_0$) of the samples were calculated using the equation

$$\Delta R/R_0 = (R–R_0)/R_0 \quad (1)$$

where ΔR is the change in resistance of sample after applying a certain strain, R is the resistance of sample at certain strain and R_0 is the initial resistance of sample without any strain. The recorded mechanical strain values are plotted against $\Delta R/R_0$ values to correlate the change in electrical resistance with mechanical strain.

Cyclic Strain Test: It was carried out by the same set of above mentioned tensile machine and electrometer used for the measurement of piezoresistive behavior. This test was performed at a speed of 0.5 mm/minute applying maximum loading strain of 7 % for 15 cycles. At the end of each loading and unloading, the test specimens were held free for 90 seconds for relaxation to start the next cycle.

3 Results and Discussion

3.1 Structural Characterization

– Figure 1 –

FTIR spectra of neat PBAT and its composite samples are presented in Figure 1. Characteristic peaks centered at 725 cm^{-1} and at 1444 cm^{-1} are due to –C–H_2 stretching and –C–H_3 bending, respectively [49, 50, 51]. Peak located at 1715 cm^{-1} corresponds to the C–O stretching vibration while peak at 1260 cm^{-1} corresponds to carbonyl group (C=O) both of which are present in ester linkage of PBAT [49, 50, 51]. Similarly, peak at 2957 cm^{-1} is associated with symmetrical −C−H stretching vibration of aromatic and aliphatic groups [49, 50] and the peaks around 1500 cm^{-1} correspond to aromatic rings [51, 52].

All of the above mentioned peaks are exhibited due to functional groups and chemical bonds present in the polymer matrix alone. Neither new bands nor significant shift of peak position in the nanocomposites compared to the neat matrix can be observed. The polymer matrix displayed exactly the same spectra as all the nanocomposites indicating the absence of any chemical interaction between filler and matrix and implying that the interaction is only of physical nature.

3.2 Morphological Characterization

– Figure 2 –

– Figure 3 –

Scanning electron microscopy (SEM) was used to analyze the fracture surface morphology of the samples and the dispersion of MWCNTs in polymer matrix. SEM micrographs presented in Figure 2a and 2b show that filler particles are uniformly dispersed throughout the polymer matrix forming an interconnected network structure. From SEM micrographs, however, any aggregation of MWCNTs and changes in the network density with higher weight fraction of filler is hardly detectable. To analyze the formed conductive network, transmission electron microscopy (TEM) and volume resistivity measurements (an indirect method) were employed. The morphology of composites can be correlated to the electrical conductivity of composites.

TEM was used to investigate the dispersion and orientation of CNTs, and network formed in polymer matrix taking a thin section of composites. TEM micrographs presented in Figure 3 show the homogeneous mixing of MWCNTs in polymer matrix with partial aggregation (highlighted in circles). The CNT particles seem to be gathered to some extent rather than completely dispersed as individuals. However, uniformly distributed interconnected individual tubes and agglomerates both contributing to form a network structure can be observed. Comparative observation of micrographs presented in Figure 3a and 3b suggests the higher agglomeration with higher filler content. The agglomeration is caused by the strong van der Waals force of attraction between filler particles.

3.3 Mechanical Characterization – Tensile Test

– Figure 4 –

– Table 1 –

Tensile stress–strain curves of the nanocomposites containing different wt.-% of filler along with that of pure PBAT are shown in Figure 4 (the data of all samples are compiled in Table 1). These curves can be differentiated with respect to tensile strength, strain at break and their initial slopes correlated with filler content. All of the composite samples break in the strain range of 105 – 530 % while the pure PBAT broke above 588 % strain showing a large plastic deformation and tensile strength of 21.5 MPa (Table 1). Neat PBAT performs highly ductile nature (elongation at break >400 %) and all of the composites perform ductile nature (elongation at break >100 %. [49]. In the high-strain range, it can be observed that the mechanical performance of the composites with respect to tensile strength as well as strain at break worsen with increasing filler content. Agglomeration of filler particles as well as formation of cracks and voids in the composite materials might have occurred with increasing filler content due to strong van der Waals force of attraction between CNT particles and their non-wetting (to some extent) by polymer matrix. In the low-strain range, however, an improving trend in stress level and tensile modulus of the composites can be observed with higher content of MWCNTs (as clearly shown in stress–strain curves in the insert of Figure 4). The increasing initial slope of stress–strain curves implies that elastic modulus of the composites increases with filler concentration in the

nanocomposites. Tensile strength of 12 MPa and strain at break of about 350 % of PBAT/10 wt.-% microcrystalline cellulose composites are reported by Giri *et al.* [49]. Moustafa *et al.* have reported a tensile strength of 11.3 MPa and strain at break of 304 % of PBAT/10 wt.-% torrefied coffee ground composites [53] while PBAT/10 wt.-% MWCNT composites of this work exhibit tensile strength and strain at break of 15.3 MPa and 105 %, respectively. Similarly, Pinheiro *et al.* has reported the values of 21.5 MPa and 710.6 % tensile strength and elongation at break, respectively, from the investigation of composites based on PBAT and 3 wt.-% octadecyl isocyanate-modified cellulose nanocrystals [54]. On the other hand, PBAT/3wt-% MWCNT composites investigated in this work possess the values of 18 MPa and 374 %, respectively. Hence, MWCNTs seem better reinforcing fillers in comparison to coffee grounds and unmodified microcrystalline cellulose despite of the opposite performance in comparison to modified cellulose nanocrystals.

3.4 Mechanical Characterization – Microindentation Test

The different parameters including corresponding standard deviations are presented in Table 2. Variation in Martens hardness (*HM*), indentation modulus (E_{IT}) and maximum indentation depth (h_{max}) of neat PBAT and the PBAT/MWCNTs nanocomposites are presented in Figure 5a. From the plot, increasing trend in the value of Martens hardness and those of indentation modulus and the decreasing trend in maximum indentation depth values with increasing filler content in nanocomposites can be observed. It suggests the reinforcement of nanocomposites by the dispersed filler particles.

– Figure 5 –

– Table 2 –

The Martens hardness values do not increase continuously with CNTs content although they are in overall increasing trend. Neat PBAT and the nanocomposites with 0.5 % filler has the lowest Martens hardness values (~6.8 N/mm^2) with highest indentation depth values (~39 μm) and indentation modulus values (~122 MPa). Martens hardness values are found to decrease at highest filler weight fractions of 10 wt.-%. It may be caused by the formation of voids, cracks and agglomerates above electrical percolation threshold and overfilling of filler particles, respectively. However, the values of indentation modulus and maximum indentation depth are in continuously increasing and decreasing trend, respectively, except in the filler concentration ≤ 1 wt.-%. The maximum Martens hardness value (12.2 N/mm^2) is recorded at 6 % filler content with maximum indentation depth of 32.4 μm and indentation modulus of 182 MPa. This value of *HM* is almost double in comparison to that of pure polymer matrix. However, the minimum indentation depth value (30.8 μm) is at 10 % filler content with maximum indentation modulus value (212 MPa). These results signify that maximum indentation depth and indentation modulus values mainly depend on filler content while *HM* values depend on energy dissipation and filler agglomeration (morphology) processes overlying the effect of filler weight fraction. The standard deviation of all parameters (*HM*, E_{IT} and h_{max}) is remarkably high at 1 % filler content after which it is in decreasing trend revealing that the rate of MWCNTs agglomeration is not so high even in 10 wt.-% filler. Compared to other PBAT composites the microindentation behavior of PBAT is the most improved by incorporating MWCNTs. At 10 wt.-% filler, adding of MWCNTs results in *HM* and E_{IT} values of 10.8 N/mm^2 and 212 MPa (in this study) compared to

8.8 N/mm^2 and 165 MPa for PBAT/microcellulose [49] and 6.0 N/mm^2 and 104 MPa for PBAT/nanocellulose [55], respectively.

Similarly, work done by elastic and plastic deformation (W_e and W_p) during microindentation test of neat PBAT and PBAT/MWCNTs nanocomposites are presented in Figure 5b. The work done by elastic and plastic deformation seems to be inversely correlated i.e. the values of work done by elastic deformation increase if the values of work done by plastic deformation decrease for lower filler fraction and in the reverse way for higher filler fraction. The values of work done by elastic deformation and that by plastic deformation with their standard deviations are presented in Table 3.

– Table 3 –

3.5 Electrical Characterization – Volume Resistivity

Volume resistivity of the composites depends on electrical percolation and state of dispersion of conductive fillers and the formation of conductive network in the polymer matrix. It is an indirect method to generate information about conductive network and the state of dispersion of filler particles. As shown in Figure 6, the composites with 0.5 wt.-% CNTs is electrical non-conductive (volume resistivity: 1.3×10^{13} Ω·cm) but that with 1 wt.-% CNTs is conductive with quite low volume resistivity (4.6×10^{5} Ω·cm). Similarly, all of the composites above 1 wt.-% CNTs are found to be electrical conductive. Volume resistivity values (Table 4) of these conductive composites show that they can be applicable for sensors [56]. Hence, the percolation threshold of PBAT/MWCNTs nanocomposites occurs between 0.5 and 1 wt.-% of MWCNTs which is a quite low percolation threshold. Agglomeration of CNT particles increases percolation threshold and affects electrical and mechanical properties of nanocomposites because these phenomena reduce the number of contacts between filler particles during the formation of conductive network.

The volume resistivity of PBAT / 1 wt.-% MWCNT composites is lower than that of PBAT / 0.5 wt.-% MWCNT composites by 8 decades. Higher filler contents just gradually decreased the volume resistivity, which confirms that a perfect conductive network has already been formed at 1 wt.-% filler concentration [6]. The corresponding values of volume resistivity at different filler content are tabulated in Table 4.

As suggested by volume resistivity values, insulator-to-conductor transition of the composites occurred between 0.5 and 1 wt.-% filler concentration . Such a transition and continuously decreasing volume resistivity value (almost levels off after 3 wt.-%) with rising filler content indicates homogeneous filler distribution throughout the matrix forming a more and more perfect conductive network. Beyond 3 wt.-% filler content, the volume resistivity corresponds to the increasing network density in the composites [48].

– Figure 6 –

– Table 4 –

Agglomeration of CNTs also contributes to the electrical conductivity; however, reduce the homogeneity in the formation of 3D conductive network throughout the matrix surface and in the cross section which is essential for the isotropic conductivity of nanocomposites. Formation of a

homogeneous network throughout the resulting composites will have more pronounced effects on their mechanical properties than individually dispersed particles or agglomerates. However, the dispersion and the conductivity of individual CNT particle cannot be correlated directly to the electrical properties of nanocomposites because other factors such as length and diameter of nanotubes, curvature, synthesis methods and conditions, mixing parameters such as mixing time and speed, temperature and pressure etc. equally affect the electrical properties of resulting nanocomposites.

3.6 Electrical Characterization – Piezoresistance

The resistance of PBAT/MWCNTs nanocomposites was measured up on increasing tensile strain. Change in electrical resistance of nanocomposites as a function of strain applied and initial resistance (R_0) is presented in Figure 7a (lower-strain regime) and Figure 7b and 7c (higher-strain regime). The nanocomposites having filler concentration above percolation threshold (i.e. 1, 3, 6 and 10 wt.-%) were taken for the measurement to investigate their piezoresistive behavior. Exponential change of $\Delta R/R_0$ values with increasingly applied strain during tensile measurement confirms the piezoresistive behavior of composite materials [14, 15]. The change in resistance with increasing strain applied was measured till sample rupture. The entire (wide) range of measurement of the nanocomposites can be deduced from the plots presented in Figure 7a, 7b and 7c. The nanocomposites with 1, 3, 6 and 10 wt.-% of MWCNTs exhibit elongation at break of 334, 219, 153 and 45 %. Increasing trend of resistance of each sample with increasing elongation tensile strain with respect to their original resistance (R_0) is observed which is caused by the disconnection of CNTs, deformation of individual CNT, resulting increasing tunneling resistance and complete or partial destruction of conducting filler network during strain application on flexible composite materials [12, 44] (as shown in Figure 7c, the breakdown of the filler network occurs at elongations very smaller than the strain at break).

Closer view of the plot in Figure 7a suggests that the composites with 1 wt.-% MWCNTs show no increase of $\Delta R/R_0$ values after 1 % strain suggesting very early damage of percolation network. However, nanocomposites with 3 wt.-% filler increases most sharply which means that CNT network is the weakest among them (excluding the 1 wt.-% composites) with a highest value of initial resistance (R_0) in comparison to other composites. Maximum $\Delta R/R_0$ values of 20 and 200 of this nanocomposite at elongation strain of 0.9 % and 7.5 %, respectively, are suggested (Figure 7a and 7b). Composites with filler concentration close to percolation threshold show higher piezoresistivity than that with higher filler concentration because network density increases with higher filler concentration after percolation and the rate of CNTs disconnection up on applied strain decreases. Meanwhile, higher stiffness with higher filler concentration decreases the stretchability of materials. The piezoresistive curve of the samples at strain ranges smaller than 1.1 % can be divided into two major regions [43, 46]. They are marked as region A and region B (and an A–B transition at about 0.6 % strain between) in Figure 7a. The region for strain higher than 1.1 % is designated as region C (Figure 7b). $\Delta R/R_0$ values increase in a linear way with respect to increasing strain in region A, where the relatively low $\Delta R/R_0$ values per % strain ranges from about 4 to about 9 % (Table 5) for 3 – 10 wt.-% MWCNT (and a value of 31 for 1 wt.-% MWCNT). Very low strain value is effective in this region to cause the resistance change and increase in resistance is caused by separation of filler particles from single or few conductive paths in this region. Rearrangement of CNTs forming new electrical paths can also

occur because of the flexible nature of PBAT. The total resistance of the composites is not only determined by nearby CNTs with direct contact but also by PBAT molecules located between neighbored CNTs which still allow tunnelling of electrons. In this region, the rate of disconnection of CNTs is slightly higher than their internal rearrangement. Similarly, deformation of individual CNT as well as partial destruction of conducting paths can be assumed in region B in which resistance tends to increase in a linear way while complete destruction and sample failure up to its rupture is occurring in region C. In region C with strain higher than 1.1 % the resistance can increase even exponentially (observed for 3 and 6 wt.-% MWCNTs) [34, 44, 46]. Both in the region B and the region C the nanocomposites having different filler fraction can be clearly distinguished (Figure 7a and 7b). In region B, the $\Delta R/R_0$ values per % strain are higher than those in region A ranging from about 90 (PBAT/ 1 wt.-% MWCNT) *via* 49 (PBAT/ 3 wt.-% MWCNT) up to about 12 (PBAT/ 6 wt.-% MWCNT), but it is about zero for the composite with the highest MWCNT content (PBAT/ 10 wt.-% MWCNT) (Table 5). This trend of piezoresistivity leads to the conclusion that the conductive network with low filler concentration (near to percolation) is easy to destruct and more sensitive to the applied strain.

– Figure 7 –

Above 0.6 % strain, the change in resistance of 10 wt.-% nanocomposite seems to be almost constant, i.e. the resistance is strain-insensitive for this nanocomposite for higher strain. It corresponds to the high network density of the CNT network, increasing stiffness and decreasing stretchability of the nanocomposites. Filler aggregation and their uneven distribution may have also occurred at higher filler concentration. These phenomena affect the flexibility and stretchability of polymer matrix. These results are in agreement with the observations from tensile test and TEM.

– Table 5 –

Hence, the nanocomposites prepared are found to be piezoresistive in nature whose sensing response can be altered by controlling the filler content as well as by limiting the applied tensile strain. Such a strain-dependent electrical response even at lower-strain regime indicates the strain-sensing capacity of these materials. High flexibility of PBAT/MWCNTs makes them applicable for low-strain deformation sensing purpose.

3.7 Electrical Characterization – Cyclic Strain Test

Reproducibility and stability of strain-sensing behavior of materials can be confirmed by the cyclic strain test. Therefore, cyclic strain test was performed using the PBAT/ 3 wt.-% MWCNTs composites (R_0 = 51.2 Ω) in addition to the static stress–strain.

– Figure 8 –

Mechanical strain of 0.5 % (just after linear change of $\Delta R/R_0$ values in Figure 7a and 7b)) and 7 % (below yield stress) were separately applied on these composites for cyclic strain experiment. The $\Delta R/R_0$ *versus* time with 0.5 % strain application in cyclic experiment decreased continuously which was independent of time and the cycles of experiment (results are not presented here). It was due to the relaxation and conditioning effect of the composites with low-strain application by which resistance of the composites decreased instead of its expected increment [14]. Figure 8 presents the plot of $\Delta R/R_0$, strain and stress *versus* time applying 7 %

strain in maximum during cyclic strain experiment. Maximum and minimum values of $\Delta R/R_0$ gradually decreased with the increasing number of cycles which is due to the irreversible detachment of adjacent CNTs with increasing strain. The largest difference of maximum and minimum $\Delta R/R_0$ values seems while moving from first to second cycle (up to 550 seconds) carried out by the minimum unrecoverable, plastic type of deformation of PBAT during the test. However, change in $\Delta R/R_0$ values seems the most stable from second to fourth and again from fifth to seventh cycles (from 500 to 3000 seconds) as shown in Figure 8b. It further decreases and again becomes stable in last few cycles with a small difference of maximum and minimum $\Delta R/R_0$ values. From closer view of Figure 8b, it is revealed that change in $\Delta R/R_0$ values is not perfectly strain controlled even in the most stable cycles regardless its overall trend. Despite of higher range of strain and stress, it seems to be constrained within 2–5 % strain and 1.5–4 MPa stress range. Hence, minute investigation of $\Delta R/R_0$ change particularly with in these strain and stress range can determine the extent of stable piezoresistive behavior of these materials.

4 Conclusion

Dispersion of MWCNTs into PBAT matrix *via* melt mixing followed by compression molding produced flexible electrical conducting and piezoresistive PBAT/MWCNTs nanocomposites with partial filler aggregation.

PBAT was found to be conductive by the incorporation of only 1 wt.-% of CNTs into it confirming a relatively low percolation threshold (between 0.5 and 1 wt.-% filler).

Analyses of FTIR spectra of the nanocomposites in comparison to that of neat polymer matrix revealed the physical filler–matrix interaction as a binding force for the formation of continuous interconnected nanocomposite morphology with partial aggregation as suggested by SEM and TEM, respectively.

Mechanical reinforcement of the PBAT by the MWCNTs was confirmed by microindentation and tensile measurements. Tensile results showed highly ductile behavior of both PBAT and resulting PBAT/MWCNTs nanocomposites.

Strain-dependent electrical response (piezoresistivity) of the composites above percolation threshold has been confirmed by the exponential increase of relative resistance change with mechanical strain signifying their strain-sensing applications tuned by filler concentration and strain range. The results of cyclic strain experiments demonstrated the stability and reproducibility of strain sensing behavior of the composites only at low-strain range.

Acknowledgements

KND and RA gratefully acknowledge the German Academic Exchange Service (DAAD) and Alexander von Humboldt (AvH) Foundation for funding their research stays, respectively, in Germany. Hai Hong Le acknowledges German Research Foundation (DFG) for the research fund (Project No.: DFG WI 2671/2-1). Anna Ivanov, Ulrike Jentzsch-Hutschenreuther, Holger Scheibner and Regine Boldt (Leibniz-Institut für Polymerforschung Dresden e.V. (IPF), Dresden, Germany) are further thanked for their supports in microcompounding, compression molding, piezoresistance measurement, and microscopy, respectively. Similarly, Andre Wutzler (Polymer Service GmbH Merseburg (PSM), Merseburg, Germany) is thanked for spectroscopic

investigation and supports in tensile test. Furthermore, the authors from Nepal also like to thank very much the foundation "Heinz-Bethge-Stiftung" in Halle/Saale, Germany ("Zukunftsfonds Nepal"), the foundation "Stiftung Akademie Mitteldeutsche Kunststoffinnovationen" (AMK) in Merseburg, Germany ("Stipendienfonds Materialwissenschaften") and Prof. Thomas Thurn-Albrecht (Martin Luther University Halle-Wittenberg, Halle/Saale, Germany) for financial funding as well as the Fraunhofer Institute for Microstructure of Materials and Systems (IMWS) in Halle/Saale, Germany for organising the German–Nepalese colloquium „Faserverstärkte Kunststoffe und nachhaltiges Bauen" (06/06/2016, Halle/Saale, Germany).

Authors Contributions

KD, BK, SK and RA performed the experiments. KD drafted the first manuscript while RL and RA played leading role in manuscript formulation. KD and RL visualised the data. RL, AD, SW made arrangements for experiments and analysis of the results. WG, SW, HL, JP and GH provided overall supervision of the research and provided critical evaluation of the results. RA was responsible for acquisition of funding.

References

1. P. Pötschke, A. R. Bhattacharyya, A. Janke, Melt mixing of polycarbonates with multiwalled carbon nanotubes: Microscopic studies on the state of dispersion, *Eur. Polym. J.* 40 (2004) 137–148. https://doi.org/10.1016/j.eurpolymj.2003.08.008.
2. J. Li, J. Kim, Percolation threshold of conducting polymer composites containing 3D randomly distributed graphite nanoplatelets, *Compos. Sci. Technol.* 67 (2007) 2114–2120. https://doi.org/10.1016/j.compscitech.2006.11.010.
3. I. Alig, T. Skipa, D. Lellinger, P. Pötschke, Destruction and formation of a carbon nanotube network in polymer melts: Rheology and conductive spectroscopy, *Polyme*r 49 (2008) 3524–3532. https://doi.org/10.1016/j.polymer.2008.05.037.
4. W. Zhang, A. A. Dehghani-Sanij, R. S. Blackburn, Carbon based conductive polymer composites, *J. Mater. Sci.* 42 (2007) 3408–3418. https://doi.org/10.1007/s10853-007-1688-5.
5. T. Villmow, S. Pegel, A. John, R. Rentenberger, P. Pötschke, Liquid sensing: Smart polymer/CNT composites, *Mater. Today* 14 (2011) 340–345. https://doi.org/10.1016/S1369-7021(11)70164-X.
6. G. Kaur, R. Adhikari, P. Cass, M. Bown, P. Gunatillake, Electrically conductive polymers and composites for biomedical application, *RSC Adv.* 5 (2015) 37553–37567. https://doi.org/10.1039/C5RA01851J.
7. M. J. Yee, N. M. Mubarak, E. C. Abdullah, Md. Khalid, R. Walvekar, R. R. Karri, S. Nizamuddin, A. Numan, 2019, Carbon nanomaterials based films for strain sensing application – A review, *Nano-Structures Nano-Objects* 18, 100312. https://doi.org/10.1016/j.nanoso.2019.100312.

8. P. Pötschke, M. H. Arnaldo, H.-J. Radusch, Percolation behavior and mechanical properties of polycarbonate composites filled with carbon black/carbon nanotube systems, *Polimery* 57 (2012) 204–211. DOI: 10.14314/polimery.2012.204.
9. M. Mičusik, M. Omastová, I. Krupa, J. Prokes, P. Pissis, E. Logakis, C. Pandis, P. Pötschke, J. Pionteck, A comparative study on the electrical and mechanical behaviour of multi-walled carbon nanotube composites prepared by diluting a masterbatch with various types of polypropylenes, *J. Appl. Polym. Sci.* 113 (2009) 2536–2551. https://doi.org/10.1002/app.30418.
10. B. Krause, P. Pötschke, E. Illin, M. Predtechenskiy, Melt mixed SWCNT–polypropylene composites with very low electrical percolation, *Polymer* 98 (2016) 45–50. https://doi.org/10.1016/j.polymer.2016.06.004.
11. P. Pötschke, S. Dudkin, I. Alig, Dielectric spectroscopy on melt processed polycarbonate–multiwalled carbon nanotube composites, *Polymer* 44 (2003) 5023–5030. https://doi.org/10.1016/S0032-3861(03)00451-8.
12. M. Amjadi, Y. J. Yoon, I. Park, 2015, Ultra-stretchable and skin-mountable strain sensors using carbon nanotubes–ecoflex nanocomposites, *Nanotechnology* 26, 375501. https://doi.org/10.1088/0957-4484/26/37/375501.
13. P. Pötschke, A. R. Bhattacharyya, A. Janke, Morphology and electrical resistivity of melt mixed blends of polyethylene and carbon nanotube filled polycarbonate, *Polymer* 44 (2003) 8061–8069. https://doi.org/10.1016/j.polymer.2003.10.003.
14. X. Tang, P. Pötschke, J. Pionteck, Y. Li, P. Formanek, B. Voit, Tuning the piezoresistive behavior of poly(vinylidene fluoride)/carbon nanotube composites using poly(methyl methacrylate), *ACS Appl. Mater. Interfaces* 12 (2020) 43125−43137. https://doi.org/10.1021/acsami.0c11610.
15. K. Ke, P. Pötschke, S. Gao, B. Voit, An ionic liquid as interface linker for tuning piezoresistive sensitivity and toughness in poly(vinylidene fluoride)/carbon nanotube composites, *ACS Appl. Mater. Interfaces* 9 (2017) 5437−5446. https://doi.org/10.1021/acsami.6b13454.
16. F. Gubbels, S. Blacher, E. Vanlathem, R. Jerome, R. Deltour, F. Brouers, P. Teyssie, Design of electrical conductive composites: Key role of the morphology on the electrical properties of carbon black filled polymer blends, *Macromolecules* 28 (1995) 1559–1566. https://doi.org/10.1021/ma00109a030.
17. N. Hu, Z. Masuda, C. Yan, G. Yamamoto, H. Fukunaga, T. Hashida, 2008, Electrical properties of polymer nanocomposites with carbon nanotube fillers, *Nanotechnology* 19, 215701. https://doi.org/10.1088/0957-4484/19/21/215701.
18. A. Wurm, D. Lellinger, A. A. Minakov, T. Skipa, P. Pötschke, R. Nicula, I. Alig, C. Schick, Crystallization of poly(ε-caprolactone)/MWCNT composites: A combined SAXS/WAXS, electrical and thermal conductivity study, *Polymer* 55 (2014) 2220–2232. https://doi.org/10.1016/j.polymer.2014.02.069.
19. K. Yang, M. Gu, Y. Guo, X. Pan, G. Mu, Effects of carbon nanotube functionalization on the mechanical and thermal properties of epoxy composites, *Carbon* 47 (2009) 1723–1738. https://doi.org/10.1016/j.carbon.2009.02.029
20. F. Du, R. C. Scogna, W. Zhou, S. Brand, J. E. Fischer, K. I. Winey, Nanotube networks in polymer nanocomposites: Rheology and electrical conductivity, *Macromolecules* 37 (2004) 9048–9055. https://doi.org/10.1021/ma049164g.

21. P. Pötschke, S. Pegel, M. Claes, D. Bonduel, A novel strategy to incorporate carbon nanotubes into thermoplastic matrices, *Macromol. Rapid Commun.* 29 (2008) 244–251. https://doi.org/10.1002/marc.200700637.
22. B. Krause, G. Petzold, S. Pegel, P. Pötschke, Correlation of carbon nanotube dispersability in aqueous surfactant solutions and polymers, *Carbon* 47 (2009) 602–612. https://doi.org/10.1016/j.carbon.2008.10.040.
23. M. Mičusik, M. Omastová, J. Pionteck, C. Pandis, E. Logakis, P. Pissis, Influence of surface treatment of multiwall carbon nanotubes on the properties of polypropylene/carbon nanotubes nanocomposites, *Polym. Adv. Technol.* 22 (2011) 38–47. https://doi.org/10.1002/pat.1745.
24. P. Pötschke, M. Abdel-Goad, I. Alig, S. Dudkin, D. Lellinger, Rheological and dielectrical characterization of melt mixed polycarbonate–multiwalled carbon nanotube composites, *Polymer* 45 (2004) 8863–8870. https://doi.org/10.1016/j.polymer.2004.10.040.
25. W. Bauhofer, J. Z. Kovacs, A review and analysis of electrical percolation in carbon nanotube polymer composites, *Compos. Sci. Technol.* 69 (2009) 1486–1498. https://doi.org/10.1016/j.compscitech.2008.06.018.
26. B. Krause, R. Boldt, L. Haussler, P. Pötschke, Ultralow percolation threshold in polyamide 6,6/MWCNT composites, *Compos. Sci. Technol.* 114 (2015) 119–125. https://doi.org/10.1016/j.compscitech.2015.03.014.
27. R. Ramasubramaniam, J. Chen, H. Liu, Homogeneous carbon nanotube/polymer composites for electrical applications, *Applied Physics Letters* 83 (2003) 2928–2930. https://doi.org/10.1063/1.1616976.
28. J. K. W. Sandler, J. E. Kirk, I. A. Kinloch, M. S. P. Shaffer, A. H. Windley, Ultralow electrical percolation threshold in carbon nanotube epoxy composites, *Polymer* 44 (2003) 5893–5899. https://doi.org/10.1016/S0032-3861(03)00539-1.
29. S. B. Eshwaran, M. R. Parsekar, A. Das, H. H. Le, S. Wiessner, K. W. Stöckelhuber, G. Schmaucks, G. Heinrich, Construction of interconnected nanostructured carbon black network: Development of highly stretchable and robust elastomeric conductors, *J. Phys. Chem. C* 119 (2015) 21723–21731. https://doi.org/10.1021/acs.jpcc.5b06629.
30. T. S. Natarajan, S. B. Eshwaran, K. W. Stöckelhuber, S. Wiessner, P. Pötschke, G. Heinrich, A. Das, Strong strain sensing performance of natural rubber nanocomposites, *ACS Appl. Mater. Interfaces* 9 (2017) 4860−4872. https://doi.org/10.1021/acsami.6b13074.
31. J. Zhao, K. Dai, C. Liu, G. Zheng, B. Wang, C. Liu, J. Chen, A comparison between strain sensing behaviors of carbon black/polypropylene and carbon nanotubes/polypropylene electrically conductive composites, *Compos. Part A – Appl. Sci. Manuf.* 48 (2013) 129–136. https://doi.org/10.1016/j.compositesa.2013.01.004.
32. A. R. Chowdhury, J. Jaksik, I. Hussain, R. Longoria III, O. Fraque, F. Cesano, D. Scerano, J. Parsons, M. J. Uddin, Multicomponent nanostructured materials and interfaces for efficient piezoelectricity, *Nano-Structures Nano-Objects* 17 (2019) 148–184. https://doi.org/10.1016/j.nanoso.2018.12.002.
33. S. Qu, S.-C. Wong, Piezoresistive behavior of polymer reinforced by expanded graphite, *Compos. Sci. Technol.* 67 (2007) 231–237. https://doi.org/10.1016/j.compscitech.2006.08.008.

34. L. Chen, G. Chen, L. Lu, Piezoresistive behavior study on finger-sensing silicone rubber/graphite nanosheet nanocomposites, *Adv. Funct. Mater.* 17 (2007) 898–904. https://doi.org/10.1002/adfm.200600519
35. K. Ding, N. Wei, Y. Zhou, Y. Wang, D. Wu, H. Liu, H. Yu, C. Zhou, J. Chen, C. Chen, Viscoelastic behavior and model simulations of poly(butylene adipate-co-terephthalate) biocomposites with carbon nanotubes: Hierarchical structures and relaxation, *J. Compos. Mater.* 50 (2016) 1805–1816. https://doi.org/10.1177/0021998315596592.
36. H.-T. Chiu, S.-Y. Huang, Y.-F. Chen, M.-I. Kuo, T.-Y. Chiang, C.-Y. Chang, Y.-H. Wang, 2013, Heat treatment effects on the mechanical properties and morphologies of poly(lactic acid)/poly(butylene adipate-co-terephthalate) blends, *Int. J. Polym. Sci.* 2013, 951696. https://doi.org/10.1155/2013/951696.
37. S. Y. Hong, S. W. Ko, H. J. Choi, J. H. Lee, Multi-walled carbon nanotube/biodegradable poly(butyleneadipate-co-terephthalate) nanocomposites and their physical characteristics, *J. Macromol. Sci. B – Physics* 51 (2012) 125–133. https://doi.org/10.1080/00222348.2011.583199.
38. R. Al-Itry, K. Lamnawar, A. Maazouz, Improvement of thermal stability, rheological and mechanical properties of PLA, PBAT and their blends by reactive extrusion with functionalized epoxy, *Polym. Degrad. Stab.* 97 (2012) 1898–1914. https://doi.org/10.1016/j.polymdegradstab.2012.06.028.
39. M. M. Reddy, S. Vivekanandhan, M. Misra, S. K. Bhatia, A. Mohanty, Biobased plastics and bionanocomposites: Current status and future opportunities, *Prog. Polym. Sci.* 38 (2013) 1653–1689. https://doi.org/10.1016/j.progpolymsci.2013.05.006.
40. T. Villmow, P. Pötschke, S. Pegel, L. Haussler, B. Kretzschmar, Influence of twin-screw extrusion conditions on the dispersion of multi-walled carbon nanotubes in a poly(lactic acid) matrix, *Polymer* 49 (2008) 3500–3509. https://doi.org/10.1016/j.polymer.2008.06.010.
41. C.-S. Wu, Antibacterial and static dissipating composites of poly(butylenes adipate-co-terepthalate) and multi-walled carbon nanotubes, *Carbon* 47 (2009) 3091–3098. https://doi.org/10.1016/j.carbon.2009.07.023.
42. S. W. Ko, M. K. Hong, B. J. Park, R. K. Gupta, H. J. Choi, S. N. Bhattacharya, Morphological and rheological characterization of multi-walled carbon nanotube/PLA/ PBAT blend nanocomposites, *Polym. Bull.* 63 (2009) 125–134. https://doi.org/10.1007/s00289-009-0072-9.
43. S. Ryu, P. Lee, J. B. Chou, R. Xu, R. Zhao, A. J. Hart, S.-G. Kim, Extremely elastic wearable carbon nanotube fiber strain sensor for monitoring of human motion, *ACS Nano* 9 (2015) 5929–5936. https://doi.org/10.1021/acsnano.5b00599.
44. S.-J. Park, J. Kim, M. Chu, M. Khine, 2016, Highly flexible wrinkled carbon nanotube thin film strain sensor to monitor human movement, *Adv. Mater. Technol.* 1, 1600053. https://doi.org/10.1002/admt.201600053.
45. S. W. Lee, J. J. Park, B. H. Park, S. C. Mun, Y. T. Park, K. Liao, T. S. Seo, W. J. Hyun, O. O. Park, Enhanced sensitivity of patterned graphene strain sensors used for monitoring subtle human body motions, *ACS Appl. Mater. Interfaces* 9 (2017) 11176−11183. https://doi.org/10.1021/acsami.7b01551.
46. Y. Lin, S. Liu, S. Chen, Y. Wei, X. Dong, L. Liu, Highly stretchable and sensitive strain sensor based on graphene–elastomer composites with a novel double-interconnected network, *J. Mater. Chem. C* 4 **(**2016) 6345–6352. https://doi.org/10.1039/c6tc01925k.

47. S.-H. Bae, Y. Lee, B. K. Sharma, H.-J. Lee, J.-H. Kim, J.-H. Ahn, Graphene-based transparent strain sensor, *Carbon* 51 (2013) 236–242. https://doi.org/10.1016/j.carbon.2012.08.048.
48. J. F. Christ, N. Aliheidaria, A. Ameli, P. Pötschke, 3D printed highly elastic strain sensors of multiwalled carbon nanotube/thermoplastic polyurethane nanocomposites, *Mater. Design* 131 (2017) 394–401. https://doi.org/10.1016/j.matdes.2017.06.011.
49. J. Giri, R. Lach, H. H. Le, W. Grellmann, J.-M. Saiter, S. Henning, H.-J. Radusch, R. Adhikari, Structural, thermal and mechanical properties of composites of poly(butylene adipate-co-terephthalate) with wheat straw microcrystalline cellulose, *Polym. Bull.* (2020), published online. https://doi.org/10.1007/s00289-020-03339-5.
50. S. Pokhrel, R. Lach, H. H. Le, A. Wutzler, W. Grellmann, H. J. Radusch, R. P. Dhakal, A. Esposito, S. Henning, P. N. Yadav, J. M. Saiter, G. Heinrich, R. Adhikari, *Macromol. Symp.* 366 (2016) 23–34. https://doi.org/10.1002/masy.201650043.
51. S. Siyamak, N. A. Ibrahim, S. Abdolmohammadi, W. Md. Z. W. Yunus, Md. A. Rahman, *Molecules* 17 (2012) 1969–1991. https://doi.org/10.3390/molecules17021969.
52. S. Mohanty, S. K. Nayak, Biodegradable nanocomposites of poly(butyleneadipate-*co*-terephthalate) (PBAT) and organically modified layered silicates, *J. Polym. Environ.* 20 (2012) 195–207. https://doi.org/10.1007/s10924-011-0408-z.
53. H. Moustafa, C. Guizani, C. Dupont, V. Martin, M. Jeguirim, A. Dufresne, Utilization of torrefied coffee grounds as reinforcing agent to produce high-quality biodegradable PBAT composites for food packaging applications, *ACS Sustainable Chem. Eng.* 5 (2017) 1906−1916. https://doi.org/10.1021/acssuschemeng.6b02633.
54. I. F. Pinheiro, F. V. Ferreira, D. H. S Souza, R. F. Gouveia, L. M. F Lona, A. R. Morales, L. H. I. Mei, Mechanical, rheological and degradation properties of PBAT nanocomposites reinforced by functionalized cellulose nanocrystals, *Eur. Polym. J.* 97 (2017) 356–365. https://doi.org/10.1016/j.eurpolymj.2017.10.026.
55. J. Giri, Wheat Stalk Micro- and Nanocellulose Based Degradable Polymer Composites: Morphological, Mechanical and Degradation Behaviour, PhD Thesis, Tribhuvan University, Kathmandu. 2020.
56. H. Pang, L. Xu, D. X. Yan, Z. M. Li, Conductive polymer structures with segregated structures, *Prog. Polym. Sci.* 39 (2014) 1908–1933. https://doi.org/10.1016/j.progpolymsci.2014.07.007.

Captions of the Figures

Figure 1: FTIR spectra of PBAT and PBAT/MWCNTs nanocomposites (the spectra are shifted along y-axis for better visibility).

Figure 2: SEM micrographs of PBAT/MWCNT nanocomposites with different filler content: 3 wt.-% MWCNT (a) and 10 wt.-% MWCNT (b).

Figure 3: TEM micrographs of PBAT/MWCNT nanocomposites with different filler content under different magnification: 3 wt.-% MWCNT (a, c) and 10 wt.-% MWCNT (b, d).

Figure 4: Tensile stress–strain curves of PBAT and the PBAT/MWCNTs nanocomposites with different filler content.

Figure 5: (a) Variation of Martens hardness (*HM*), indentation modulus (E_{IT}) and indentation depth (h_{max}) and (b) variation of work done by elastic deformation (W_e) and plastic deformation (W_p) of PBAT/MWCNTs nanocomposites as a function of filler content.

Figure 6: Plot of volume resistivity *vs.* filler content of PBAT/MWCNT nanocomposites.

Figure 7: Piezoresistive behavior of PBAT/MWCNTs nanocomposites (a) at lower-strain range and (b, c) higher-strain range.

Figure 8: Cyclic strain test of PBAT/3 wt.-% MWCNT composites at wide regime (a) and close regime (b).

Tables

Table 1: Mechanical properties of PBAT and the PBAT/MWCNTs nanocomposites determined by tensile test.

Sample	Tensile modulus (MPa)	Tensile strength (MPa)	Strain at break (%)
Neat PBAT	115.8 ± 10.2	21.5 ± 4.5	588 ± 152
PBAT / 0.5 wt.-% MWCNT	107.9 ± 4.6	21.2 ± 0.5	530 ± 11
PBAT / 1 wt.-% MWCNT	112.4 ± 4.6	18.7 ± 0.9	467 ± 26
PBAT / 3 wt.-% MWCNT	145.0 ± 4.5	18.0 ± 0.6	374 ± 19
PBAT / 6 wt.-% MWCNT	162.6 ± 4.8	16.5 ± 0.5	251 ± 26
PBAT / 10 wt.-% MWCNT	195.7 ± 16.5	15.3 ± 1.8	105 ± 12

Table 2: Mechanical properties of PBAT and the PBAT/MWCNTs nanocomposites determined by microindentation test.

Sample	HM (N/mm^2)	E_{IT} (MPa)	h_{max} (µm)
Neat PBAT	6.84 ± 0.30	122.4 ± 6.8	38.56 ± 0.85
PBAT / 0.5 wt.-% MWCNT	6.78 ± 0.12	121.4 ± 2.8	38.74 ± 0.33
PBAT / 1 wt.-% MWCNT	8.46 ± 0.52	116.8 ± 9.0	38.94 ± 1.18
PBAT / 3 wt.-% MWCNT	8.20 ± 0.19	152.4 ± 5.4	35.22 ± 0.40
PBAT / 6 wt.-% MWCNT	12.18 ± 0.30	181.7 ± 4.3	32.41 ± 0.39
PBAT / 10 wt.-% MWCNT	10.76 ± 0.26	211.9 ± 6.6	30.75 ± 0.37

Table 3: Work done by elastic and plastic deformation (W_e and W_p) of PBAT and the PBAT/MWCNTs nanocomposites determined by microindentation test.

Sample	W_e (nJ)	W_p (nJ)
Neat PBAT	2864 ± 121	1082 ± 23
PBAT / 0.5 wt.-% MWCNT	2899 ± 42	982 ± 10
PBAT / 1 wt.-% MWCNT	3075 ± 182	948 ± 11
PBAT / 3 wt.-% MWCNT	2459 ± 104	1091 ± 84
PBAT / 6 wt.-% MWCNT	2226 ± 27	1049 ± 18
PBAT / 10 wt.-% MWCNT	1965 ± 40	1168 ± 30

Table 4: Electrical volume resistivity (including standard deviations) of PBAT and the PBAT/MWCNTs nanocomposites.

Sample	Volume resistivity (Ω·cm)
Neat PBAT	$8.8\times10^{13} \pm 6.4\times10^{12}$
PBAT / 0.5 wt.-% MWCNT	$1.3\times10^{13} \pm 5.6\times10^{12}$
PBAT / 1 wt.-% MWCNT	$4.6\times10^{5} \pm 2.7\times10^{5}$
PBAT / 3 wt.-% MWCNT	$3.5\times10^{3} \pm 6.0\times10^{3}$
PBAT / 6 wt.-% MWCNT	$1.3\times10^{3} \pm 1.4\times10^{4}$
PBAT / 10 wt.-% MWCNT	$1.6\times10^{2} \pm 9.3\times10^{2}$

Table 5: $\Delta R/R_0$ per % strain of PBAT and some PBAT/MWCNTs nanocomposites according to the regions in Figure 7a.

Sample	A–B transition (% strain)		$\Delta R/R_0$ per % strain	
	Range	Intersection point	Region A	Region B
PBAT / 1 wt.-% MWCNT	0.48 – 0.53	0.49	31.22 ± 5.26	89.55 ± 1.45
PBAT / 3 wt.-% MWCNT	0.34 – 0.75	0.60	7.90 ± 0.37	48.99 ± 1.35
PBAT / 6 wt.-% MWCNT	0.48 – 0.64	0.53	4.07 ± 0.07	12.02 ± 0.12
PBAT / 10 wt.-% MWCNT	0.48 – 0.64	0.63	9.38 ± 0.19	ca. 0

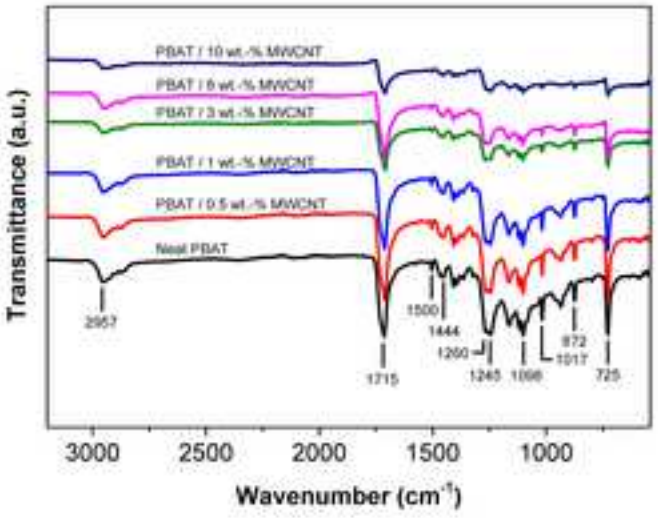

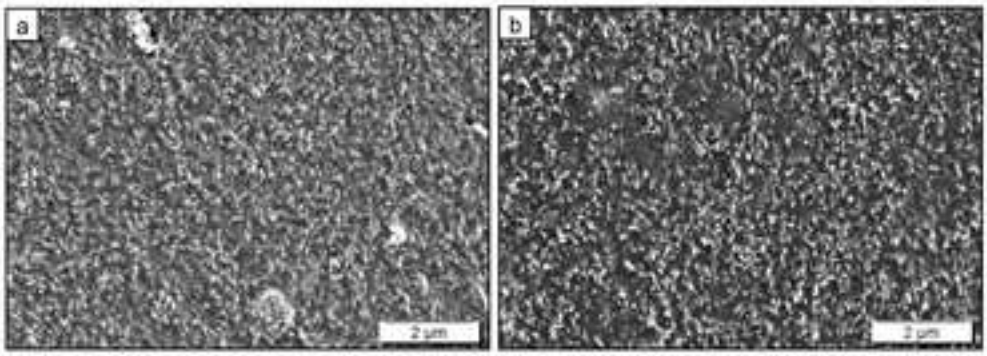

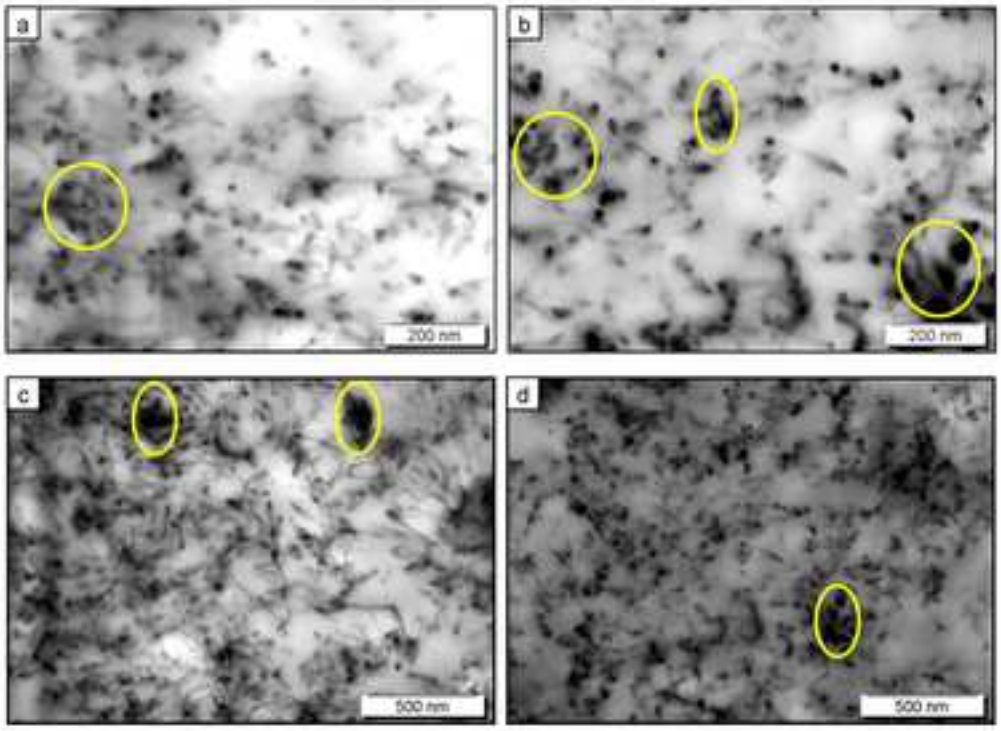

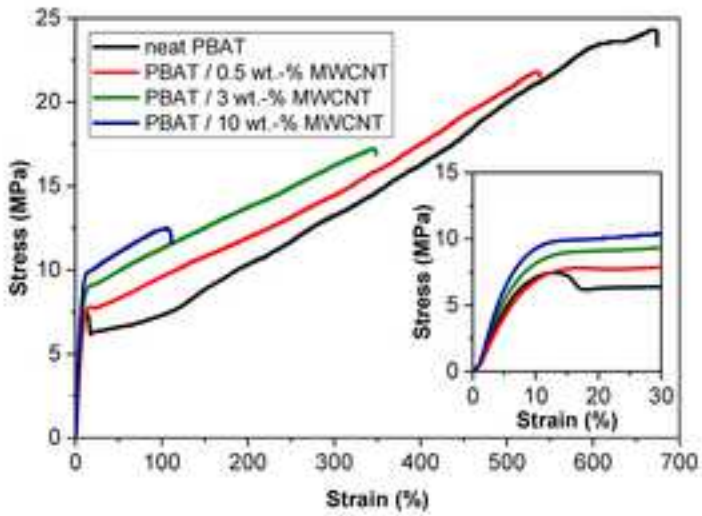

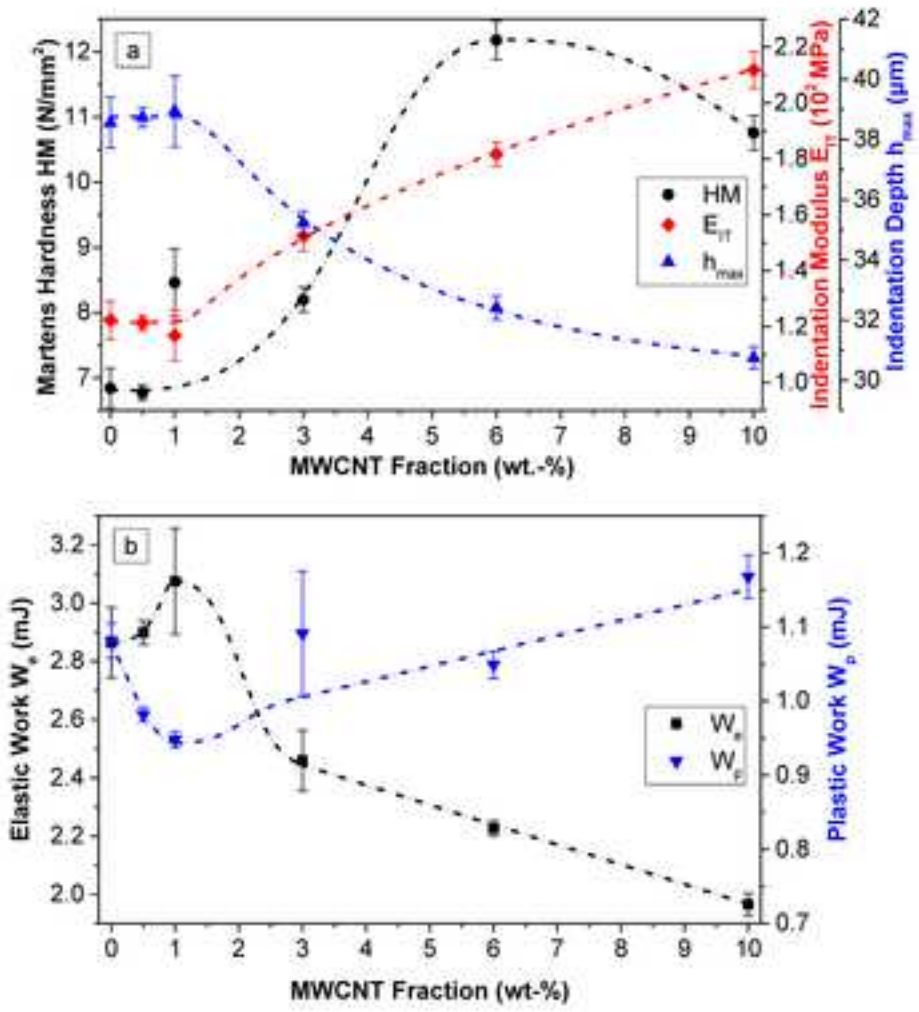

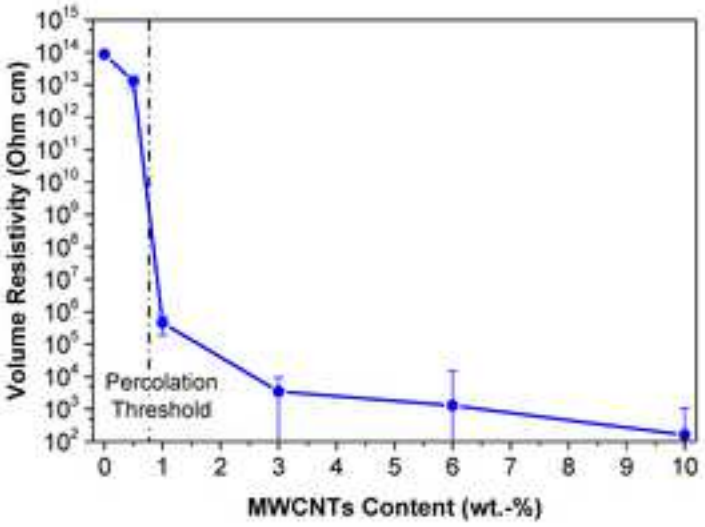

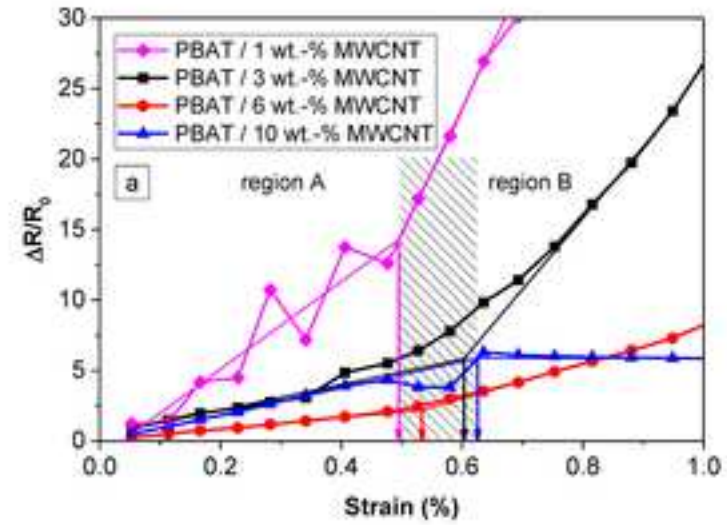

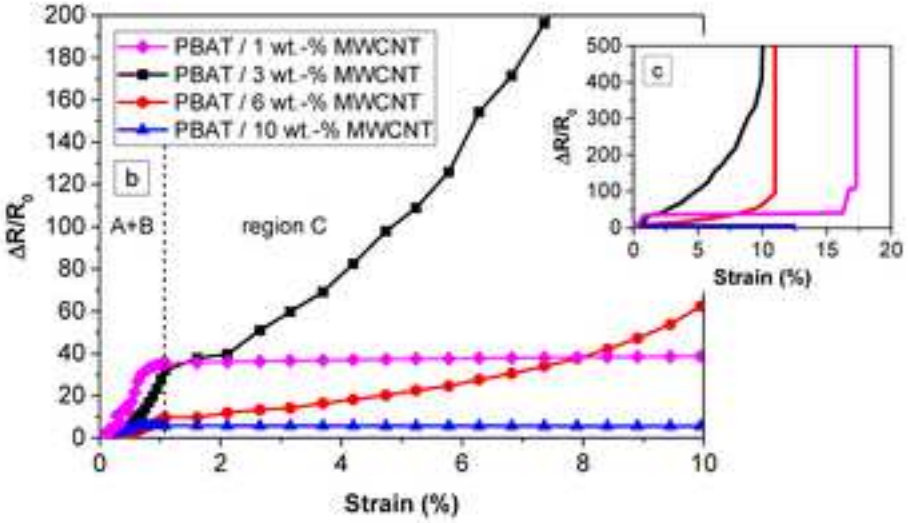

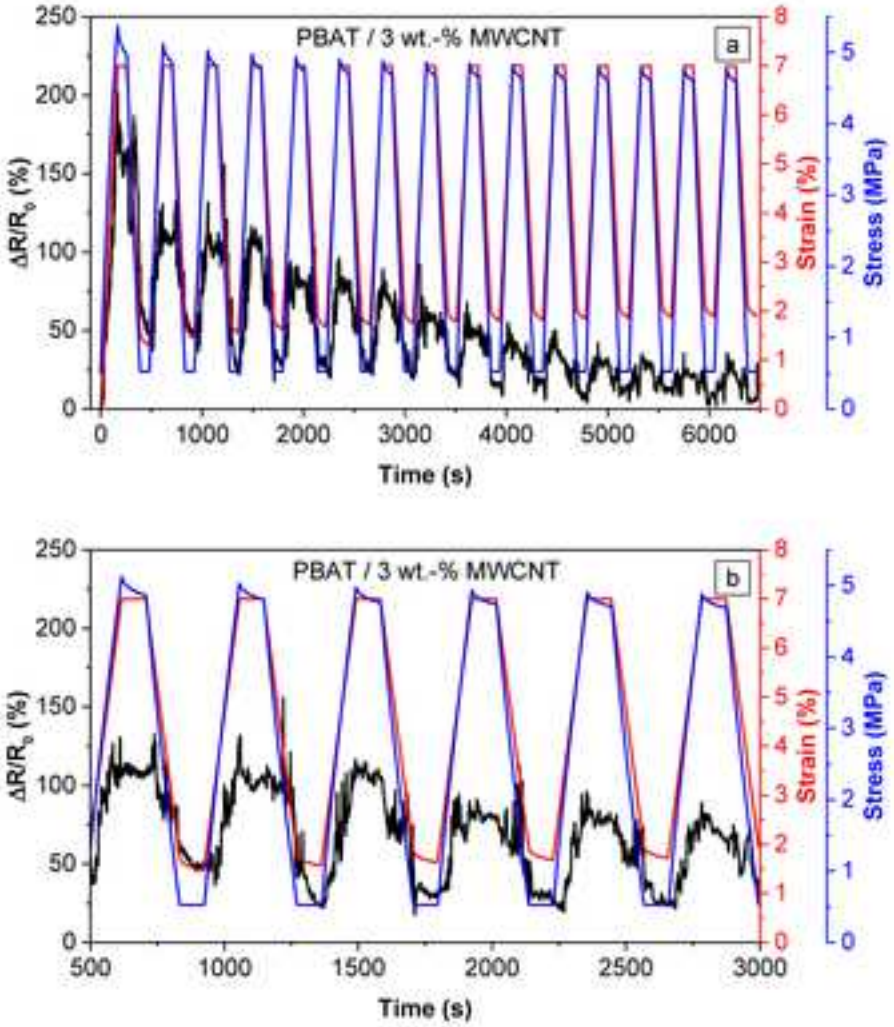

Graphical abstract